Title

Crystallinity Effects in Sequentially Processed and Blend-Cast Bulk-Heterojunction Polymer/Fullerene Photovoltaics

Journal

The Journal of Physical Chemistry C, 118(32)

ISSN

1932-7447

Authors

Zhang, Guangye
Huber, Rachel C
Ferreira, Amy S
et al.

Publication Date

2014-08-14

DOI

10.1021/jp5054315

Peer reviewed

THE JOURNAL OF PHYSICAL CHEMISTRY C

Article

pubs.acs.org/JPCC

Crystallinity Effects in Sequentially Processed and Blend-Cast Bulk-Heterojunction Polymer/Fullerene Photovoltaics

Guangye Zhang,[†,§] Rachel C. Huber,[†,§] Amy S. Ferreira,[†,§] Shane D. Boyd,[‡] Christine K. Luscombe,[‡] Sarah H. Tolbert,*[,†,⊥] and Benjamin J. Schwartz*[,†]

[†]Department of Chemistry and Biochemistry, University of California, Los Angeles, 607 Charles E. Young Drive East, Los Angeles, California 90095-1569, United States

[‡]Materials Science and Engineering Department, University of Washington, Box 352120, Seattle, Washington 98195-2120, United States

[⊥]Department of Materials Science and Engineering, University of California, Los Angeles, Los Angeles, California 90095, United States

Supporting Information

ABSTRACT: Although most polymer/fullerene-based solar cells are cast from a blend of the components in solution, it is also possible to sequentially process the polymer and fullerene layers from quasi-orthogonal solvents. Sequential processing (SqP) not only produces photovoltaic devices with efficiencies comparable to the more traditional bulk heterojunction (BHJ) solar cells produced by blend casting (BC) but also offers the advantage that the polymer and fullerene layers can be optimized separately. In this paper, we explore the morphology produced when sequentially processing polymer/fullerene solar cells and compare it to the BC morphology. We find that increasing polymer regioregularity leads to the opposite effect in SqP and BC BHJ solar cells. We start by constructing a series of SqP and BC solar cells using different types of poly(3-hexylthiophene) (P3HT) that vary in regioregulary and polydispersity combined with [6,6]-phenyl-C_{61}-butyric-acid-methyl-ester (PCBM). We use grazing incidence wide-angle X-ray scattering to demonstrate how strongly changes in the P3HT and PCBM crystallinity upon thermal annealing of SqP and BC BHJ films depend on polymer regioregularity. For SqP devices, low regioregularity P3HT films that possess more amorphous regions allow for more PCBM crystallite growth and thus show better photovoltaic device efficiency. On the other hand, highly regioregular P3HT leads to a more favorable morphology and better device efficiency for BC BHJ films. Comparing the photovoltaic performance and structural characterization indicates that the mechanisms controlling morphology in the active layers are fundamentally different for BHJs formed via SqP and BC. Most importantly, we find that nanoscale morphology in both SqP and BC BHJs can be systematically controlled by tuning the amorphous fraction of polymer in the active layer.

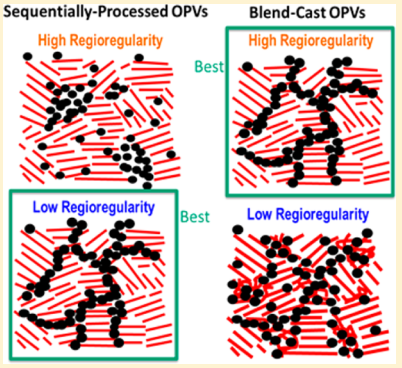

I. INTRODUCTION

In recent years, dramatic progress has been made in the field of organic photovoltaics (OPVs),[1,2] resulting in power conversion efficiencies (PCEs) of polymer/fullerene devices surpassing 10%.[3−6] This achievement is based mostly on traditional blend-cast (BC) bulk heterojunctions (BHJs),[7] in which an electron-donating polymer and electron-accepting fullerene are mixed together in a solution that is used to cast the active layer of the organic solar cell. The resulting film is then typically thermally or solvent annealed to promote phase separation of the polymer and fullerene, resulting in a conductive network for both electrons and holes as well as intermixed regions where a majority of charge separation occurs.[8−17] The morphology of BC BHJ films is dictated by multiple factors, including the donor/acceptor miscibility, the propensity of one or both materials to crystallize,[16,18−21] the relative solubilities of the two materials in the casting solution, the drying kinetics of the film, the presence of any solvent additives,[22−26] etc. Because the nm-scale morphology depends on so many of the details of how the film is cast, the device performance of BC BHJ solar cells is hypersensitive to the processing kinetics of the active layer.[7] Thus, for any new set of OPV materials, an Edisonian approach involving the fabrication of hundreds of BC devices is needed to find the processing conditions that lead to the optimal morphology and best device performance.

An alternative approach to preparing polymer/fullerene active layers for photovoltaic applications has been to sequentially process the polymer and fullerene components in separate steps by depositing the materials from quasi-orthogonal solvents.[27] This sequential processing (SqP) technique has been studied by several groups in both polymer−fullerene[28−36] and small molecule−fullerene sys-

Received: June 2, 2014
Revised: July 14, 2014
Published: July 18, 2014

   dx.doi.org/10.1021/jp5054315 | J. Phys. Chem. C 2014, 118, 18424−18435

tems.[37] It is well established that, even though the fullerene is deposited on top of the polymer layer, the resultant film still has a significant amount of fullerene dispersed through the polymer layer,[38] particularly after thermal annealing.[39−41] Not only are the PCEs of devices fabricated via SqP comparable to or better than the more traditional BC devices[36,37,42−48] but the SqP method also provides several distinct advantages that could make it the preferred route for large-scale fabrication of polymer-based photovoltaics. First, films produced via SqP have a more reproducible morphology because SqP does not rely on kinetic control of the nm-scale structure, resulting in devices that behave more consistently (cf. Figure 1, below).[27,42,49] Second, since the two materials are deposited separately, one can optimize or otherwise deliberately alter the donor material (e.g., by chemical doping) either before[50−52] or after[53] it has been processed, without unwanted chemistry occurring with the electron-accepting material. Third, sequentially processed films are guaranteed to have a fullerene network that is connected to the top of the film, avoiding issues with undesirable vertical phase separation that necessitate the use of an inverted device geometry. Finally, many solubility issues can be bypassed since one can separately choose optimal solvents for the donor and acceptor materials.[37,54] Thus, the SqP technique potentially opens the photovoltaic field to a variety of donor and acceptor materials that once were not usable due to compatibility issues between solvents and materials.

Although it is clear that the BHJ morphology of films produced via SqP is generally similar to that of BC films in that the fullerene is dispersed throughout the polymer, a variety of experiments have suggested that the details of the nm-scale distribution of the polymer and fullerene differ between the two processing techniques. For example, ultrafast spectroscopic studies have shown that the dynamics of exciton quenching and polaron production are different in optically matched sequentially processed and BC films made from the workhorse materials poly(3-hexylthiophene) (P3HT) and [6,6]-phenyl-C_{61}-butyric-acid-methyl-ester (PCBM).[55] Moreover, nominally matched sequentially processed and BC photovoltaic devices show different behaviors upon thermal annealing.[42,48,49,56] Thus, the most important issues concerning solar cells fabricated via SqP are precisely how the nm-scale morphology is different from that in BC films and what factors control the extent and distribution of fullerene interpenetration into the polymer underlayer.

In this paper, we work to build an understanding of the fullerene distribution in P3HT/PCBM BHJ solar cells produced via both SqP and blend-casting. Our approach is to take advantage of a series of P3HTs with a narrow molecular weight distribution and precisely controlled regioregularity that allow us to explore how changing specific attributes of the polymer leads to differences in both the BHJ architecture and in the PV performance of sequentially procssed and BC devices. It is well-known that polymer regioregularity and polydispersity index (PDI) can have dramatic effects on the photovoltaic performance of BC BHJs,[57−63] and here we extend these studies to sequentially processed devices, focusing in particular on how regioregularity affects the morphology and device performance of thermally annealed P3HT/PCBM active layers. In agreement with previous suggestions, we first find that PCBM deposited by sequential processing preferentially penetrates into the amorphous regions of the P3HT underlayer, leaving the crystalline regions of the polymer essentially intact.[40,56] We then show that too much polymer crystallinity is actually unfavorable for SqP photovoltaic devices because too little fullerene can penetrate around the crystallites, leading to over-phase separation of the polymer and fullerene. In contrast, BC devices show the opposite behavior: highly regioregular (and thus more crystalline) P3HT provides better efficiencies than BC devices made from lower regioregularity P3HTs. We thus conclude that sequentially processed and BC BHJ devices require different materials properties to achieve formation of their ideal active layer morphologies.

II. EXPERIMENTAL SECTION

The key feature underpinning this work is the successful synthesis of P3HT with well-defined regioregularity and extremely narrow PDI.[64] In what is described below, we compare the behavior of three different batches of P3HT: commercial P3HT purchased from Rieke Metal Inc. (BASF Sepiolid P100), which we denote as LR P3HT, and two in-house batches synthesized with 98% regioregularity and average molecular weights of about 16 kDa (PDI = 1.18) and 37 kDa (PDI = 1.19), denoted as HR P3HTs, where LR and HR stand for low regioregularity and high regioregularity, respectively. The full characteristics of the three batches we focus on here are summarized in Table 1. Additional details about polymer batch information and our in-house batch purification procedures, as well as a high regioregularity 50 kDa in-house-synthesized batch, can be found in the Supporting Information (SI).

Table 1. Characteristics of P3HT Used in This Work

	M_n (kDa)	regioregularity	PDI	mobility (SCLC) ($cm^2\ V^{-1}\ s^{-1}$)
low RR (LR) P3HT	∼50−60	∼94%	∼2.20	1.6×10^{-5}
16k high RR (HR) P3HT	15.9	98%	1.18	3.4×10^{-5}
37k high RR (HR) P3HT	36.9	98%	1.19	1.3×10^{-5}

For measurements of the optical properties and for structural characterization of our BHJ films, we prepared a series of sequentially processed active layers by first spinning a ∼110 nm thick layer of P3HT from *o*-dichlorobenzene, and then we subsequently deposited PCBM layers from either 5%, 10% or 15% weight/volume dichloromethane solutions on top by spin-coating, leading to P3HT/PCBM films with a total thickness in the range of 155 to 185 nm. We then prepared BC active layers (∼175 nm thick) by spinning a composite P3HT:PCBM (1:0.9 weight ratio) solution from *o*-dichlorobenzene at 1000 rpm for 60 s. Identical active layers were used to fabricate photovoltaic devices with Ca/Al evaporated on top as the cathode.

We note that no slow drying of solvent or solvent vapor treatments were performed on either the sequentially processed or BC devices, even though such treatments are necessary to optimize the PCE for the P3HT/PCBM materials combination. Instead, we chose our spin-coating parameters to provide us with completely dry films after spinning. We made this choice to eliminate drying kinetics, which can cause marked variations in the performance of BC devices.[42,65] In this way, we were able to maintain our focus on how polymer properties such as regioregularity and molecular weight control variations in morphology and device performance.

dx.doi.org/10.1021/jp5054315 | J. Phys. Chem. C 2014, 118, 18424−18435

The detailed procedures of our film and device fabrication and characterization also can be found in the SI.

III. RESULTS AND DISCUSSION

In this section, we begin by discussing the hole mobility of the three polymer batches we investigate in this work (Table 1). Although we find that polymer regioregularity and molecular weight do slightly affect hole transport, the differences we observe are subtle, suggesting that BHJ morphology is a much larger factor in determining device performance than the raw hole mobility of the bare polymer. We then use these different polymer batches to fabricate SqP and BC solar cells and demonstrate that polymer regioregularity has the opposite effect for the two different processing techniques in terms of photovoltaic device efficiency. This result can be understood through a series of morphological studies, including thin film absorption, fluorescence quenching, and grazing incidence wide-angle X-ray scattering measurements, which allow us to directly explore the structural changes that occur upon thermal annealing and to define the optimal conditions needed to create ideal morphologies for BC and SqP solar cells.

A. Device Physics of BC and SqP Solar Cells Made from Different P3HTs. *1. Hole Mobility of Different P3HTs.* Many groups have examined how the mobilities of P3HT films are controlled by different polymer properties, such as the regioregularity and/or molecular weight.[58,59,66−70] The generally accepted trend is that increasing regioregularity and increasing molecular weight lead to higher charge carrier mobilities,[68] although most such measurements are made on field-effect transistors (FETs).[71] Since the direction of charge transport for photovoltaic devices is perpendicular to that in FETs, we chose to examine the carrier mobilities in our P3HT batches in sandwich-structure devices so that our measurements would be directly relevant for the performance of these materials in solar cells.

We fabricated diodes from each batch of P3HT using an architecture of ITO/PEDOT:PSS/P3HT/Au to ensure that the majority carriers in the device are holes. We then fit the corresponding dark $J-V$ curves using the space-charge limited current (SCLC) model, yielding the mobilities listed in Table 1 (details of the device fabrication, diode performance, and SCLC fitting procedure are given in the SI). The 16k HR P3HT shows the highest hole mobility, a bit over twice that of the LR P3HT, which has a molecular weight of roughly 50 kDa. Surprisingly, the 37k HR P3HT shows the lowest mobility, even though it has the same regioregularity as the 16k HR batch but a higher molecular weight. These results indicate that P3HT hole mobility has a complex dependence on both regioregularity and molecular weight. We note, however, that the hole mobilities for all three P3HT batches all fall within a factor of 2.6. This suggests that when these different P3HTs are employed in photovoltaic devices, all else being equal, differences in hole mobility are not likely to explain any significant difference in device performance. This allows us to use these batches to understand how differences in regioregularity and molecular weight result in morphology differences that affect solar cell performance and how these differences depend on the processing route chosen to make the BHJ active layer.

2. Comparing the Performance of SqP and BC Devices with Controlled P3HT Regioregularity and Fullerene Composition. To determine the effect of polymer regioregularity/crystallinity on the performance of the solar cells with different active-layer processing methods, we constructed working photovoltaic devices with both SqP and BC active layers from both the 16k HR P3HT and LR P3HT batches. Figure 1 demonstrates the $J-V$ characteristics of the devices

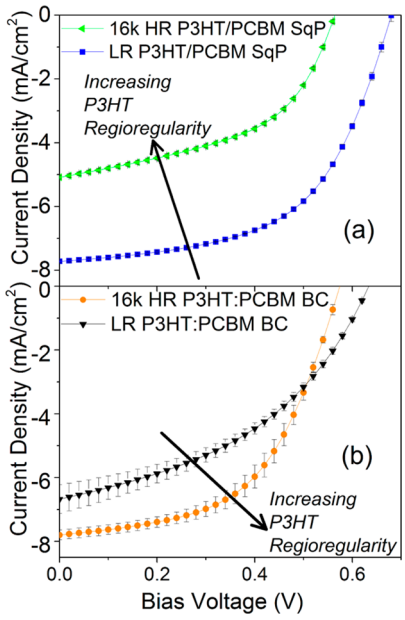

Figure 1. Current density versus applied bias for (a) ITO/poly(ethylene-dioxythiophene):poly(styrenesulfonic acid)-(PEDOT:PSS)/P3HT/PCBM/Ca/Al sequentially processed solar cells and (b) ITO/PEDOT:PSS/P3HT:PCBM/Ca/Al BC BHJ solar cells under AM-1.5 illumination. The SqP active layer was made by spinning 5 mg/mL PCBM solution onto a 110 nm P3HT underlayer (see SI). All of the SqP and BC films were thermally annealed at 150 °C for 20 min prior to deposition of the cathode. The error bars show 1 standard deviation in measurements over at least 12 independent devices. Although error bars can be clearly seen in panel (b), they are comparable to or smaller than the symbols used to plot the data in panel (a), indicating that SqP devices are more reproducible than BC devices.

under AM 1.5 solar illumination; the data plotted are the average $J-V$ curves from at least 12 separate devices, and the error bars (which in some cases are smaller than the symbols used to plot the data) are ±1 standard deviation. The full $J-V$ characteristics for all the devices we studied are detailed in Table 2. The data show clearly that, even though SqP devices require one more spin-coating step than BC devices, SqP devices can be fabricated far more reproducibly. This is because SqP avoids the kinetic sensitivity of the BHJ morphology that is inherent with BC processing.[42]

The most interesting result from Figure 1 is the fact that the two P3HT batches show opposite performance trends, depending on the processing method used to make the devices. The SqP solar cells made with LR P3HT show $J-V$ characteristics similar to those published previously,[27] with average open circuit voltage V_{oc} = 0.68 V, short circuit current J_{sc} = 7.2 mA cm^{-2}, fill factor FF = 56% and PCE = 2.9%. The HR P3HT batch, however, makes poorer SqP devices with J_{sc} values of only ∼5.1 mA cm^{-2}, and PCE of only ∼1.4%. In contrast, the HR P3HT:PCBM BC devices have a significantly higher J_{sc} and ∼40% higher PCE compared to the BC devices fabricated with LR P3HT. Thus, the way polymer regioregularity/crystallinity affects device performance is not a

dx.doi.org/10.1021/jp5054315 | J. Phys. Chem. C 2014, 118, 18424−18435

Table 2. Summary of Device Parameters

	V_{oc} (V)	J_{sc} (mA/cm^2)	FF	PCE (%)	n_{ideal} (dark $J-V$)	R_{seires} (Ω cm^2)	R_{shunt} ($\times 10^5$ Ω cm^2)
37k HR P3HT/PCBM(5 mg/mL) SqP	0.56 ± 0.01	5.98 ± 0.06	0.44 ± 0.02	1.48 ± 0.07	1.62 ± 0.03	11.2 ± 2.2	13.0 ± 0.3
16k HR P3HT/PCBM(5 mg/mL) SqP	0.56 ± 0.01	5.08 ± 0.06	0.50 ± 0.01	1.43 ± 0.02	1.62 ± 0.03	8.8 ± 0.7	7.8 ± 0.0
LR P3HT/PCBM(5 mg/mL) SqP	0.68 ± 0.01	7.72 ± 0.04	0.56 ± 0.01	2.92 ± 0.02	1.43 ± 0.02	10.6 ± 0.3	20.8 ± 0.4
37k HR P3HT/PCBM(10 mg/mL) SqP	0.53 ± 0.01	5.67 ± 0.26	0.51 ± 0.01	1.52 ± 0.09	1.88 ± 0.03	12.3 ± 2.2	12.6 ± 0.0
16k HR P3HT/PCBM(10 mg/mL) SqP	0.54 ± 0.01	4.02 ± 0.29	0.50 ± 0.03	1.09 ± 0.10	1.64 ± 0.04	10.7 ± 2.1	8.7 ± 0.0
LR P3HT/PCBM(10 mg/mL) SqP	0.64 ± 0.01	8.21 ± 0.19	0.57 ± 0.01	2.97 ± 0.03	1.40 ± 0.04	10.9 ± 2.1	14.8 ± 0.2
37k HR P3HT/PCBM(15 mg/mL) SqP	0.51 ± 0.01	5.15 ± 0.27	0.48 ± 0.02	1.26 ± 0.12	2.09 ± 0.05	9.1 ± 1.9	9.5 ± 0.0
16k HR P3HT/PCBM(15 mg/mL) SqP	0.52 ± 0.01	3.34 ± 0.27	0.47 ± 0.02	0.82 ± 0.08	1.64 ± 0.05	18.3 ± 1.9	10.0 ± 0.0
LR P3HT/PCBM(15 mg/mL) SqP	0.64 ± 0.01	7.93 ± 0.39	0.52 ± 0.02	2.63 ± 0.06	1.43 ± 0.05	10.8 ± 2.0	82.2 ± 21
16k HR P3HT:PCBM BC	0.58 ± 0.01	7.80 ± 0.15	0.53 ± 0.03	2.39 ± 0.14	1.51 ± 0.02	11.2 ± 1.5	22.6 ± 0.0
LR P3HT:PCBM BC	0.64 ± 0.01	6.68 ± 0.45	0.42 ± 0.01	1.79 ± 0.07	1.65 ± 0.07	6.9 ± 1.4	7.4 ± 0.1

simple material property, but instead depends on the route via which the active BHJ layer is processed.

To understand why changing the polymer regioregularity leads to opposite changes in performance for SqP and BC devices, we performed a series of control experiments to verify that the performance changes we observed did not result from changes in the polymer molecular weight or the polymer fullerene composition of the active layer. Figure 2 and Table 2

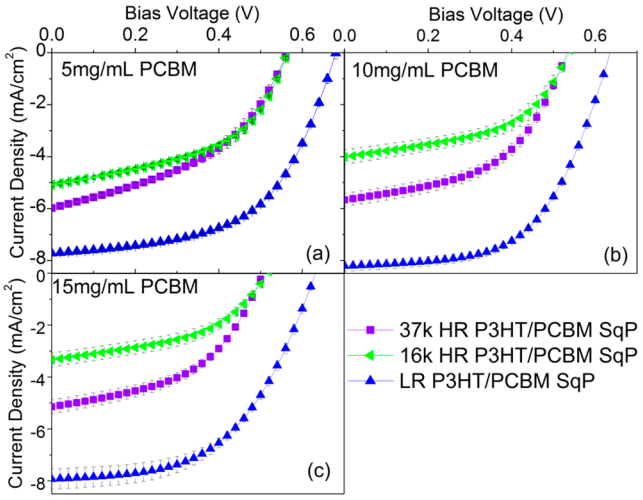

Figure 2. Effect of molecular weight, regioregularity and film composition on the $J-V$ characteristics of P3HT/PCBM devices made via SqP. LR P3HT (blue up-triangles) and two HR P3HTs with different molecular weights, 37 kDa (violet squares) and 16 kDa (green left triangles), are used as the underlayers. All P3HT underlayers were kept at ∼110 nm. Three different concentrations of PCBM (5 mg/mL, 10 mg/mL and 15 mg/mL) were spun on top of the P3HT underlayers from DCM and the corresponding $J-V$ curves are shown in panels (a), (b), and (c), respectively. The total thicknesses of the active layers are 155, 169, and 185 nm with increasing PCBM solution concentration, respectively. All samples were annealed at 150 °C for 20 min before deposition of the Ca/Al cathode. The error bars show 1 standard deviation for measurements over at least 12 independent devices.

summarize the $J-V$ characteristics of SqP solar cells made from the 16k HR P3HT (green triangles) and LR P3HT (blue squares), as well as the 37k HR P3HT (violet squares). The in-house synthesized 37k HR P3HT batch has the same high regioregularity and low PDI as the 16k HR P3HT, but a molecular weight closer to that of the commercial LR P3HT. The V_{oc} and FF of the 37k HR batch are similar to the 16k HR P3HT, but the overall PCE is higher, mainly due to increased J_{sc}. However, even though increasing the molecular weight improves the device performance, we see that the LR P3HT still shows superior performance for devices fabricated by SqP. Thus, for SqP devices, the overall performance is governed more by the degree of P3HT regioregularity than the polymer molecular weight.

In addition to polymer regioregularity, the performance of OPVs also depends sensitively on the overall polymer:fullerene composition,[43,72] a factor that is directly controlled using the ratio of polymer to fullerene in the casting solution in BC processing. In SqP, by contrast, the composition is indirectly controlled by the relative solution concentrations and spin speeds used to deposit each component of the active layer. Figure 2 thus illustrates the change in SqP solar cell performance with different polymer:fullerene compositions. In these experiments, we fixed the thickness of the P3HT underlayer and increased the concentration of the PCBM solution spun on top. We find that, with increasing fullerene loading in SqP active layer, the LR P3HT-based devices show only slight variations in J_{sc}, with an optimal polymer/fullerene composition obtained when the PCBM overlayer is spun from a 10 mg/mL solution.[27] In contrast, the performance of the SqP devices based on HR P3HT continually decreases with increased PCBM loading. Thus, not only does increased P3HT regioregularity lead to poorer SqP device performance, the results also imply that the introduction of extra fullerene cannot be accommodated in preformed high-RR P3HT underlayers.

We also have performed identical experiments exploring the changes in device performance for different batches of P3HT with different fullerene compositions for BC devices. Since similar studies have been published previously in the literature,[72−74] our results are shown in the SI. We find, in agreement with the literature, that increased P3HT regioregularity is beneficial to BC device performance. Surprisingly, however, we find that, for BC devices made from the 16k HR P3HT, the optimal P3HT:PCBM weight ratio is 1:1.3, significantly higher than the 1:0.9 optimal ratio typically seen in the literature (with lower regioregular, commercially available P3HT). Thus, for the HR-P3HT, the trend in fullerene loading for optimal BC devices also goes in the opposite direction as that for SqP devices.

3. Effects of Polymer Regioregularity on BC and SqP Device Physics. To begin our exploration of why polymer regioregularity has opposite effects on solar cells fabricated via BC and SqP, we measured the dark $J-V$ curves of the SqP and

dx.doi.org/10.1021/jp5054315 | J. Phys. Chem. C 2014, 118, 18424−18435

BC solar cells discussed above; the results are summarized in Figure 3 and Table 2.

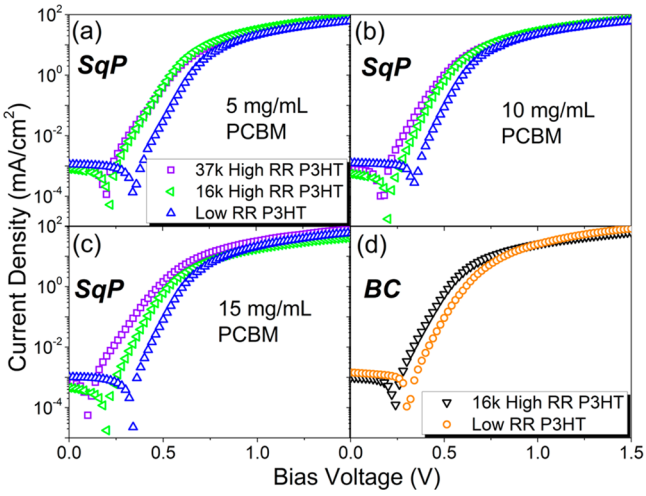

Figure 3. Dark $J-V$ characteristics of the same SqP devices in Figure 2 and the same BC devices in Figure 1.

Perhaps the most interesting parameter to consider for purposes of this study is the dark ideality factor. Typically the dark ideality factor falls into the range between 1 and 2, although numbers outside this range have been reported mainly due to resistivity effects.[75,76] Within the range of 1 and 2, a larger ideality factor is considered as a strong indication of increased trap-assisted recombination in the device, whereas lower ideality factors are more reflective of bimolecular recombination.[77−79] We derived the ideality factors for our SqP and BC devices in Table 2 from the slope of the linear regions in Figure 3; we find that the ideality factors mirror the trends in device performance. For SqP devices with a given fullerene concentration, the ideality factors for devices based on LR P3HT are consistently lower than those fabricated with HR P3HTs. For BC devices, the opposite is true: the HR P3HT-based devices exhibit lower ideality factors than the LR P3HT-based devices. This implies that the polymer/fullerene interfacial trap distribution is quite different for the different BHJ morphologies formed through the two processing techniques.

Based on the data presented above and the structural data presented below, we offer the following picture for the changes in device physics with polymer regioregularity. Low P3HT regioregularity typically leads to more amorphous regions in BHJ films made from the traditional blend-casting method. Since there are fewer crystalline polymer regions and more structural disorder, there is a greater degree of trap-assisted recombination. In contrast, increasing the polymer regioregularity in SqP devices causes the ideality factor to increase no matter what fullerene loading is used. This suggests that pre-existing P3HT underlayers can support only a certain amount of PCBM, an amount presumably limited by the fraction of the polymer that lies within amorphous regions. Thus, increasing the polymer regioregularity decreases the available space for fullerene intercalation, so that increased regioregularity leads to poorer device performance. If one tries to compensate for this by increasing the fullerene concentration in SqP devices, large-scale phase separation of the fullerene from the highly crystalline polymer network occurs (see SI), leading to an increase in the fraction of structural traps and thus trap-assisted recombination, as seen with the increased ideality factor.

Finally, we note that the devices made with different batches of P3HT also have slightly different V_{oc}'s. The trend that V_{oc} is lower in both SqP and BC devices with HR P3HT correlates with the concomitant red-shift of the absorption spectrum, described further below. This red-shift results from the fact that the highest occupied molecular orbital (HOMO) increases slightly in energy with increasing regioregularity of P3HT because of enhanced delocalization.[80,81] It is also known that increasing the amount of trap-assisted recombination can result in decreased V_{oc}, particularly for devices with carrier mobilities similar to those used here.[82] Since we indeed find that HR P3HT shows more trap-assisted recombination in the SqP devices but less in BC devices, this can help us explain the fact that the V_{oc} decrease observed in BC devices (0.06 V) is smaller than that seen in SqP devices (>0.1 V): the recombination effect goes in the same direction as the HOMO level effect in determining V_{oc} for the SqP devices while the two effects partially compensate in BC devices.

B. Understanding How P3HT Crystallinity Affects the BHJ Architecture for SqP and BC OPVs. Now that we have shown that polymer regioregularity causes opposite effects in SqP and BC photovoltaic device performance, we turn in this section to study how regioregularity affects the active layer morphology in both SqP and BC films. To this end, we perform thin-film absorption, fluorescence quenching, and grazing incidence wide-angle X-ray scattering (GIWAXS) to examine differences in the active layer morphologies formed via SqP and BC.

1. UV−vis and PL of SqP and BC Active Layers with Different P3HT Regioregularities. Figure 4 shows the UV−visible absorption spectra of pure P3HT films from each of the different polymer batches as well as spectra of all of the SqP and BC active layers discussed above. The spectra of the pure LR P3HT (dashed curve) is shifted to the blue by about 13 nm compared to the HR P3HT (solid and dash-dotted curve), and the relative intensity of the vibronic peaks is also different. Both Spano[83,84] and others[85−87] have shown that the ratio of the intensity of the 0−0 peak (A_{0-0}) to the 0−1 peak (A_{0-1}) is directly related to the intermolecular coupling and thus the crystallinity of P3HT. For our polymer batches, we observe higher A_{0-0}/A_{0-1} ratios for the 37k and 16k HR P3HT than for the LR P3HT, indicating higher crystallinity in the HR P3HT films. The slight decrease of A_{0-0}/A_{0-1} for the 37k HR P3HT sample compared to the 16k sample indicates the crystallinity of the polymers is slightly affected by their molecular weights. Despite this, the data suggest the polymer regioregularity is the most important factor in determining the film crystallinity.

The symbols in Figure 4a−c show the absorption spectra of the same P3HT films after sequential deposition of a PCBM overlayer and subsequent thermal annealing at 150 °C for 20 min. We find that for all three P3HT batches, the SqP film absorption is nearly identical to that of the pure polymer, indicating that the fullerene incorporated into the film through sequential processing induces little disruption to the crystalline polymer domains.

The band seen near 340 nm in the BHJ films in Figure 4 arises primarily from the absorption of PCBM, although there is some residual absorption of P3HT at this wavelength. Since the pure P3HT absorption at 340 nm is nearly identical for all three polymer batches, we can use the 340 nm peak intensity to roughly evaluate the PCBM content in each of the SqP films

dx.doi.org/10.1021/jp5054315 | J. Phys. Chem. C 2014, 118, 18424−18435

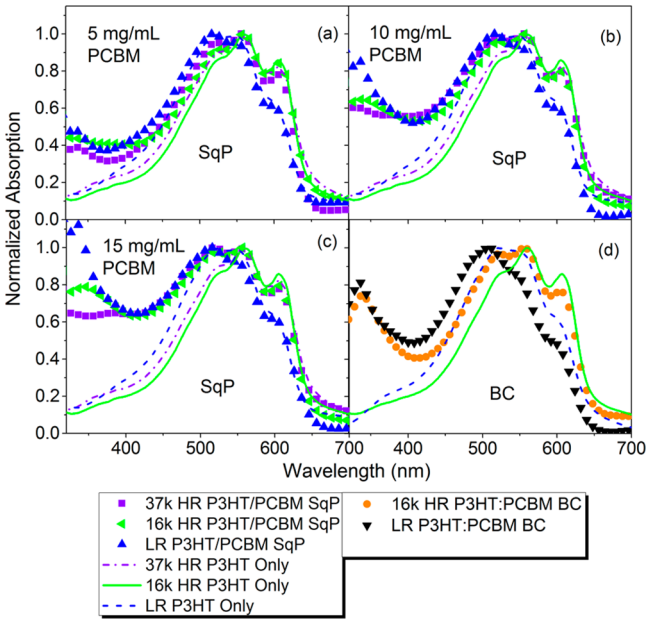

Figure 4. UV−visible absorption spectra of thin films made from different batches of pure P3HT (solid dashed and dash-dotted lines) and SqP P3HT/PCBM films (symbols) made from the same P3HTs with (a) 5 mg/mL PCBM, (b) 10 mg/mL PCBM, and (c) 15 mg/mL PCBM spun on top; and (d) BC P3HT:PCBM films made from the same P3HTs. The pure P3HT films were 110 nm thick in all cases. All films were thermally annealed at 150 °C for 20 min and the spectra in all panels are normalized to the highest polymer optical density (i.e., highest OD to the red of 490 nm) for ease of comparison.

(but see ref 42). For SqP films with the PCBM overlayer cast from a 5 mg/mL solution, the fullerene content of the films is quite similar, suggesting that any of the underlayer films can accommodate the relatively modest amount of fullerene provided by the dilute solution. For SqP active layers produced using more concentrated PCBM solutions, however, the HR P3HT samples show much weaker fullerene absorption than LR P3HT sample. This confirms that higher crystallinity polymers are less able to incorporate fullerene during SqP; if there are fewer amorphous regions into which PCBM can penetrate into the bulk of the film, more of the fullerene is likely to simply spin off during deposition of the overlayer. In the SI, we show optical micrographs of these films whose absorption spectra are shown in Figure 4; the films made from HR P3HT batches with high PCBM concentrations spun on top show fullerene aggregates/crystals at the μm-length scale, consistent with the idea that sequentially processed high crystallinity films cannot accommodate significant fullerene loadings.

Unlike the sequentially processed films, whose absorption spectra do not change upon the addition of fullerene, the vibronic features in the absorption spectra of P3HT:PCBM BC films (Figure 4d) are strongly altered by the presence of fullerene. For the LR P3HT flim, the vibronic peaks have a dramatcially decreased intensity relative to the pristine P3HT, even after 20 min of thermal annealing at 150 °C. This suggests for LR P3HT, the presence of fullerene hinders the crystallization of P3HT during both the spin-coating and thermal annealing processes. In the case of the HR P3HT:PCBM BC films, although the A_{0-1}/A_{0-0} ratio does not remain constant as observed in the seqentially processed films, it does not decrease as strongly as in the LR P3HT:PCBM BC BHJ films. Thus, this data suggests that even in BC films, the inherent crystallinity of HR P3HT can be better retained than that of LR P3HT.

In addition to UV−visible spectroscopy, we also performed a series of photoluminescence (PL) quenching experiments of SqP and BC P3HT:PCBM films made from the different polymer batches, the results of which are shown in Figure 5.

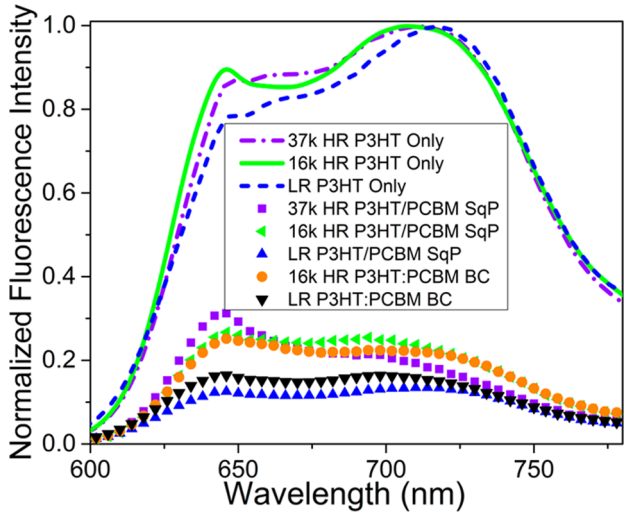

Figure 5. Photoluminescence (PL) spectra of thin films made from pure P3HTs (same as Figure 4a), SqP P3HT/PCBM films (same as Figure 4a) and P3HT:PCBM BC films (same as Figure 4d). The measured PL intensities were divided by each film's optical density at 530 nm, the excitation wavelength used in this experiment, and then normalized to the highest PL value (that of the pure 16k HR P3HT film) to best illustrate the extent of PL quenching in the different samples.

The PL spectra of the pure P3HT polymer films are similar, with only slight differences in the relative height of the 0−0 peak near 650 nm that reflect the changes in intermolecular coupling with the degree of polymer crystallinity,[83] in agreement with the UV−visible data in Figure 4. Overall, the trends observed in BC and SqP films are very similar. HR samples show less PL quenching in all cases compared to LR samples, a result that indicates that the equilibrium (i.e., post-annealing) extent of polymer−fullerene mixing at the molecular scales is driven primarily by polymer regioregularity and not by the processing method. This result is particularly interesting in light of the facts that HR material produces the best BC devices while LR material gives SqP devices with the highest efficiency. The results thus emphasize how the same level of atomic-scale mixing must be accompanied by very different nanoscale architectures using the two different processing methods. For a separation-based process like BC, strong separation appears to drive the formation of an optimized nanoscale architecture. By contrast, for a mixing-based process like SqP, a strong driving force for mixing is needed to create that same ideal architecture.

2. Morphology of SqP and BC Films with Different Batches of P3HT Measured by X-ray Diffraction. To directly investigate how changes in the P3HT regioregularity affect the polymer and fullerene crystallinity for the different processing routes used to make BHJs, we performed a series of two-dimensional (2-D) grazing incidence wide-angle X-ray scattering (GIWAXS) measurements. For these experiments, we used all the same processing methods described above but

dx.doi.org/10.1021/jp5054315 | J. Phys. Chem. C 2014, 118, 18424−18435

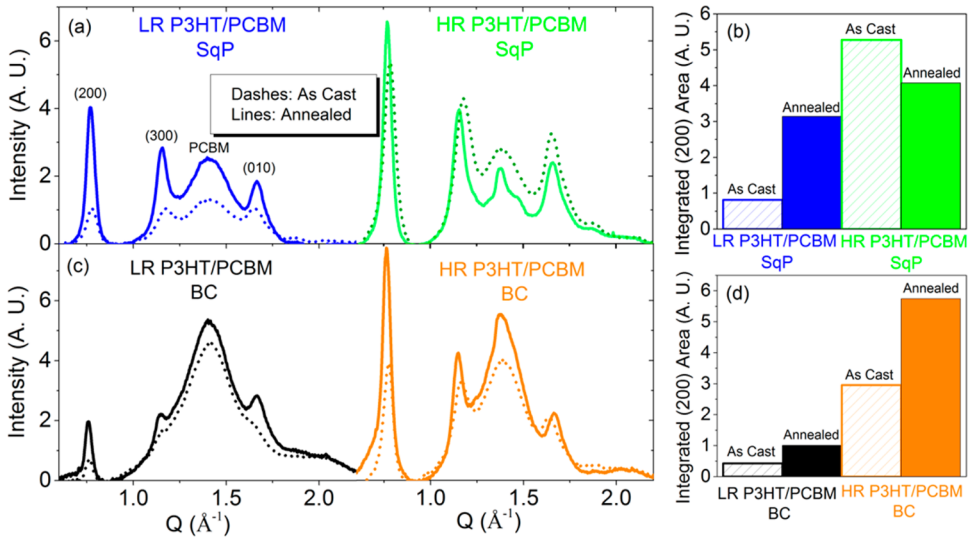

Figure 6. (a) Radially integrated 2-D GIWAXS intensities for P3HT/PCBM sequentially processed active layers cast on a silicon substrate for LR and HR P3HT. In each case, the P3HT film thickness was 110 nm, and the PCBM overlayer was spun from a 5 mg/mL solution. (b) Integrated peak area for the (200) polymer peak for SqP. (c) Integrated GIWAXS intensity for P3HT/PCBM BC films. (d) Integrated peak area for the (200) polymer peak for BC-BHJ films. Dashed lines indicate as-cast films and solid lines are after 20 min of thermal annealing at 150 °C for both (a) and (c).

Table 3. Summary of Parameters from GIWAXS

	(200) peak position ($Å^{-1}$)	(200) peak area (A.U.)	(200) fwhm[a] (10^{-2} $Å^{-1}$)	(010) peak position ($Å^{-1}$)	(010) peak area (A.U.)	(010) fwhm[a] (10^{-2} $Å^{-1}$)
LR P3HT/PCBM SqP as cast	0.778	8.1	6.6	1.657	10.9	10.7
LR P3HT/PCBM SqP annealed	0.770	31.4	5.6	1.664	13.5	7.7
16k HR P3HT/PCBM SqP as cast	0.787	52.8	6.9	1.655	35.4	10.0
16k HR P3HT/PCBM SqP annealed	0.770	40.8	5.1	1.662	23.3	8.9
LR P3HT:PCBM BC as cast	0.766	4.3	4.6	1.627	15.7	14.9
LR P3HT:PCBM BC annealed	0.759	10.1	3.9	1.663	29.8	12.0
16k HR P3HT:PCBM BC as cast	0.776	29.6	5.5	1.634	20.1	11.6
16k HR P3HT:PCBM BC annealed	0.761	57.4	5.1	1.663	15.0	8.1

[a]The full width at half-maximum (fwhm) is inversely proportional to the coherence length, which is an estimate of the length over which the ordered crystalline packing is maintained.

instead spun the active layer materials onto silicon substrates. Our GIWAXS measurements were performed at the Stanford Synchrotron Radiation Light Source on beamline 11−3 using a wavelength of 0.9742 Å. We should note that the absolute diffraction intensities cannot be compared between SqP and BC data sets because of different beam intensities during separate experimental runs; the relative intensities for a single processing method, however, can be meaningfully compared within each set. Below, we show only radially integrated scattering data; the full 2-D GIWAXS diffraction patterns are given in the SI. The results from our GIWAXS measurement are summarized in Figure 6 and Table 3.

2.1. Polymer Diffraction in SqP Samples. We begin our discussion by examining the P3HT (200) peaks, located between 0.77 and 0.79 $Å^{-1}$, which arise from P3HT lamellar interchain stacking. The (200) peak is mostly distributed in the out-of-plane direction due to the dominant "edge-on" orientation of the P3HT chains relative to the substrate (see SI). For the as-cast SqP films (dashed curves), the integrated (200) peak area of the 16k HR P3HT is more than six times higher than that of the LR P3HT. The peak center of the HR P3HT is also positioned at higher Q than that of LR P3HT, which indicates more compact lamellar stacking for the HR P3HT. We note that in polymeric systems, the broadening of X-ray scattering peaks results from disorder in the polymer domains, rather than from the finite size of crystallites as seen in crystalline materials.[16,88,89] Thus, the fwhm or coherence lengths reported here are those derived from the Scherrer equation, even though the size of the crystalline polymer domains are likely smaller. In Table 3, the two P3HT batches show similar fwhm for the (200) peaks. From this data, we conclude that a larger fraction of the as-cast HR P3HT-based SqP samples is crystalline, but the crystallites in both films have similar coherence lengths. The HR samples also show closer packing than the LR P3HT-based samples, a fact that likely arises from increased ordering of the hexyl tails in the HR films.

The literature suggests that thermal annealing of SqP films serves the dual roles of facilitating fullerene diffusion into the polymer underlayer and helping to further crystallize amorphous polymer domains.[41,90] Indeed, the solid curves in

dx.doi.org/10.1021/jp5054315 | J. Phys. Chem. C 2014, 118, 18424−18435

Figure 6a show that, for both batches of P3HT, annealing causes the (200) peaks to become sharper, indicating the formation of more ordered P3HT domains with larger structural coherence lengths. The change in the intensity of the (200) peak area upon thermal annealing, however, is quite different for the different SqP P3HT batches. For the LR P3HT, annealing increases the peak area by over a factor of 3, a result similar to previous studies on BC devices. Surprisingly, the peak area for the HR P3HT actually decreases upon thermal annealing, indicating that annealing this particular polymer/fullerene blend makes the film *less* crystalline. Further investigation reveals that unlike the LR P3HT, where annealing causes essentially no shift of the (200) peak, the HR P3HT (200) peak center shifts slightly toward lower Q, indicating the d-spacing between the lamellar planes becomes larger after annealing. This likely results from a small amount of PCBM diffusing into the P3HT crystallites.

We next turn to investigate the trends of the (010) peak, which corresponds to the polymer $\pi-\pi$ stacking direction and is therefore important for charge delocalization and transport. We find that the same general trends with polymer regioregularity and thermal annealing observed for the (200) peak also hold in the (010) direction for our SqP films. For the LR P3HT, however, the increase in (010) peak area upon annealing is less dramatic than that observed for the (200) peak, but the decrease in (010) peak width upon annealing is greater. These data thus indicate that in the (010) direction, thermal annealing predominantly affects the crystalline coherence length, likely from improvements in $\pi-\pi$ stacking upon annealing. For the HR SqP P3HT samples, we saw that the diffraction peaks decrease in intensity upon thermal annealing and that the decrease of the (010) peak area is slightly greater than the decrease seen in the (200) direction. Overall, the change in both peak width and peak area are qualitatively similar for the (010) and (200) peaks, suggesting that for SqP samples made with HR P3HT, diffusion of PCBM into the film reduces the extent of crystallinity in a fairly isotropic manner, likely by creating amorphous polymer regions where the fullerene can reside. This is in contrast to the LR samples, where annealing of paracrystalline disorder and fullerene diffusion are coupled in a more complex manner.

Clearly, the most significant difference between the two batches of SqP P3HT films is the total amount of amorphous polymer. We believe that a certain amorphous fraction is necessary for the PCBM to penetrate into sequentially processed films. Even though the HR P3HT starts out highly crystalline with few amorphous regions, the thermally induced mixing that drives PCBM into the polymer underlayer actually disrupts the P3HT network by creating additional amorphous regions upon incorporation. This produces the surprising result of a polymer/fullerene sample that becomes less crystalline upon annealing.

2.2. Polymer Diffraction in BC Samples. In as-cast BC films, the BHJ is formed with the presence of both the polymer and the fullerene, leading to a different morphology than the case of SqP. Based on shifts in diffraction peaks, we find that there is more PCBM intercalation into the BC P3HT network in both the (200) and (010) directions for as-cast BC films relative to SqP films. After thermal annealing, a large amount of the PCBM in BC films is pushed out of the $\pi-\pi$ interlayers, as evidenced by a sizable shift toward high Q for the (010) π-stacking peak. This (010) shift upon annealing does not occur with the SqP films. But perhaps more importantly, thermal annealing causes the crystallinity of both the HR and LR P3HT batches to increase when the film is prepared via BC. This provides one reason why the BC devices made from HR P3HT show superior performance compared to those made via SqP.

Another factor that could contribute to the change in device performance with regioregularity is the shape of the polymer crystallites. The widths of the (200) and (010) peaks indicate that the length of the HR P3HT crystallites are shorter than those of the LR P3HT in the (200) direction but longer in the (010) direction. Since the charge carrier transport in the $\pi-\pi$ direction is important to the mobility of holes in OPV devices,[88] one might expect hole extraction in HR P3HT active layers to be more efficient than that in LR P3HT samples. Since the hole mobility in P3HT:PCBM blend films is typically lower than the electron mobility,[91] the HR P3HT provides a better mobility-matched active layer and therefore a device with higher fill factor[92] than the LR P3HT BC device, as seen in Figure 1.

2.3. Fullerene Diffraction in SqP and BC Samples. In addition to the changes in the crystallinity of the different batches of P3HT, Figure 6 also shows that thermal annealing leads to changes in the crystallinity of the PCBM. For example, the PCBM diffraction (at $q \approx 1.4$ Å^{-1}) in the LR P3HT SqP film shows a significant increase in intensity upon thermal annealing, but the peak remains broad. This is consistent with the formation of many small PCBM crystallites upon thermally annealing SqP LR P3HT films. In contrast, thermal annealing dramatically sharpens the PCBM peaks in the SqP films made with HR P3HT. This indicates that, in highly crystalline P3HT, there are too few amorphous regions in which the PCBM can mix with the polymer, so that annealing forces the fullerenes to crystallize into fewer, but significantly larger, domains that are not consistent with an ideal BHJ architecture. These large domains may be accompanied by isolated fullerenes at grain boundaries, but those isolated fullerenes do not diffract and do not create effective conductive paths for photogenerated electrons. This hypothesis is supported by optical images, shown in the SI, which reveal that, after thermal annealing, there is optically visible phase separation of the PCBM in the HR P3HT film.

All of these results make sense in the context of two ideas: first, that PCBM is miscible and mobile only in the amorphous regions of P3HT films,[40,42,89,93−96] and second, that P3HT only fully crystallizes in the absence of PCBM. The LR P3HT clearly possesses more amorphous regions as-cast, so in SqP films, there is ample opportunity for thermal annealing to cause PCBM to diffuse into the polymer underlayer and form semicrystalline aggregates, as well as for some of the previously amorphous P3HT regions to crystallize. In highly crystalline as-cast polymers, on the other hand, there are almost no suitable amorphous spaces available for PCBM incorporation in SqP devices, so the polymer must partially disorder to make room for fullerene incorporation. Even with this disordering, the majority of the fullerene is still forced to aggregate into large, highly crystalline domains because it cannot mix into the already-crystalline regions of the polymer. In the case of BC films, the high propensity of the polymer to crystallize is important to help drive the phase separation of the polymer and the fullerene. In low regioregularity polymers, the P3HT cannot phase separate as easily, so an ideal interpenetrating BHJ network cannot be formed.

dx.doi.org/10.1021/jp5054315 | J. Phys. Chem. C 2014, 118, 18424−18435

IV. CONCLUSIONS

In summary, we have found that the effects of changing polymer regioregularity and thus crystallinity on active layer morphology and the photovoltaic device performance differ dramatically based on how the active layer is formed. PCBM disperses only into the amorphous regions after sequential processing onto P3HT films, so that controlling the amount of the amorphous phase has a direct impact on the subsequent device performance. SqP of P3HT with too high a polymer regioregularity results in highly crystalline films into which fullerenes cannot easily incorporate even after thermal annealing, leading to unfavorably large scale polymer/fullerene phase separation. SqP films made from P3HT with lower regioregularity possess more amorphous regions, which leads to a better polymer/fullerene network and thus more efficient solar cells. The effect of polymer crystallinity is reversed, however, if the active layer is fabricated through the traditional blend-cast method. The presence of PCBM in the mixed solution prevents P3HT from forming a highly crystalline network. Therefore, more highly regioregular P3HT is favorable because of its stronger propensity to crystallize.

This work has revealed a fundamental mechanism difference for the formation of BHJ active layer morphology between SqP and BC. All of the structural and device performance data show that SqP and BC do not produce films with the same polymer/fullerene morphology and that different materials parameters affect the film morphology in different ways for the two processing methods. This suggests that the two processing techniques are complementary and that the appropriate choice of which processing method to use to achieve high efficiency solar cells depends on the details of the particular batch of polymer and fullerene being used.

■ ASSOCIATED CONTENT

Supporting Information

Details of device fabrication procedures for both photovoltaic devices and hole-only diodes, $J-V$ curves of different P3HT/PCBM compositions, device $J-V$ characteristics, details of SCLC modeling for extracting hole mobilities of the pure P3HTs, photoluminescence measurement, 2-D GIWAXS diffractograms, and optical images taken on SqP P3HT/PCBM films. This material is available free of charge via the Internet at http://pubs.acs.org.

■ AUTHOR INFORMATION

Corresponding Authors

*E-mail: tolbert@chem.ucla.edu.

*E-mail: schwartz@chem.ucla.edu.

Author Contributions

§G.Z., R.C.H., and A.S.F. all contributed equally to this work.

Notes

The authors declare no competing financial interest.

■ ACKNOWLEDGMENTS

This work was supported the Center for Molecularly Engineered Energy Materials (MEEM), an Energy Frontier Research Center (EFRC) funded by the U.S. Department of Energy (DOE), Office of Science, Office of Basic Energy Sciences (BES) under Contract Number DE-AC06-76RLO-1830 (device studies, X-ray diffraction, manuscript preparation). Additional support was provided by the National Science Foundation under Grants CHE-1112569 (optical studies) and DMR-1407815 for the polymer synthesis. Portions of this research were carried out at the Stanford Synchrotron Radiation Lightsource, a Directorate of SLAC National Accelerator Laboratory and an Office of Science User Facility operated for the U.S. Department of Energy Office of Science by Stanford University.

■ REFERENCES

(1) Deibel, C.; Dyakonov, V. Polymer−Fullerene Bulk Heterojunction Solar Cells. *Rep. Prog. Phys.* **2010**, *73*, 096401.

(2) Helgesen, M.; Søndergaard, R.; Krebs, F. C. Advanced Materials and Processes for Polymer Solar Cell Devices. *J. Mater. Chem.* **2010**, *20*, 36.

(3) He, Z.; Zhong, C.; Su, S.; Xu, M.; Wu, H.; Cao, Y. Enhanced Power-Conversion Efficiency in Polymer Solar Cells Using an Inverted Device Structure. *Nat. Photonics* **2012**, *6*, 591−595.

(4) Li, G.; Zhu, R.; Yang, Y. Polymer Solar Cells. *Nat. Photonics* **2012**, *6*, 153−161.

(5) You, J.; Chen, C.-C.; Hong, Z.; Yoshimura, K.; Ohya, K.; Xu, R.; Ye, S.; Gao, J.; Li, G.; Yang, Y. 10.2% Power Conversion Efficiency Polymer Tandem Solar Cells Consisting of Two Identical Sub-Cells. *Adv. Mater.* **2013**, *25*, 3973−3978.

(6) You, J.; Dou, L.; Yoshimura, K.; Kato, T.; Ohya, K.; Moriarty, T.; Emery, K.; Chen, C.-C.; Gao, J.; Li, G.; et al. A Polymer Tandem Solar Cell with 10.6% Power Conversion Efficiency. *Nat. Commun.* **2013**, *4*, 1446.

(7) Yu, G.; Gao, J.; Hummelen, J. C.; Wudl, F.; Heeger, A. J. Polymer Photovoltaic Cells: Enhanced Efficiencies via a Network of Internal Donor-Acceptor Heterojunctions. *Science* **1995**, *270*, 1789−1791.

(8) Kim, Y.; Choulis, S. A.; Nelson, J.; Bradley, D. D. C.; Cook, S.; Durrant, J. R. Device Annealing Effect in Organic Solar Cells with Blends of Regioregular poly(3-Hexylthiophene) and Soluble Fullerene. *Appl. Phys. Lett.* **2005**, *86*, 63502.

(9) Ayzner, A. L.; Wanger, D. D.; Tassone, C. J.; Tolbert, S. H.; Schwartz, B. J. Room to Improve Conjugated Polymer-Based Solar Cells: Understanding How Thermal Annealing Affects the Fullerene Component of a Bulk Heterojunction Photovoltaic Device. *J. Phys. Chem. C* **2008**, *112*, 18711−18716.

(10) Collins, B. A.; Gann, E.; Guignard, L.; He, X.; McNeill, C. R.; Ade, H. Molecular Miscibility of Polymer−Fullerene Blends. *J. Phys. Chem. Lett.* **2010**, *1*, 3160−3166.

(11) Chen, D.; Nakahara, A.; Wei, D.; Nordlund, D.; Russell, T. P. P3HT/PCBM Bulk Heterojunction Organic Photovoltaics: Correlating Efficiency and Morphology. *Nano Lett.* **2011**, *11*, 561−567.

(12) Parnell, A. J.; Cadby, A. J.; Mykhaylyk, O. O.; Dunbar, A. D. F.; Hopkinson, P. E.; Donald, A. M.; Jones, R. A. L. Nanoscale Phase Separation of P3HT PCBM Thick Films As Measured by Small-Angle X-Ray Scattering. *Macromolecules* **2011**, *44*, 6503−6508.

(13) Bartelt, J. A.; Beiley, Z. M.; Hoke, E. T.; Mateker, W. R.; Douglas, J. D.; Collins, B. A.; Tumbleston, J. R.; Graham, K. R.; Amassian, A.; Ade, H.; et al. The Importance of Fullerene Percolation in the Mixed Regions of Polymer-Fullerene Bulk Heterojunction Solar Cells. *Adv. Energy Mater.* **2013**, *3*, 364−374.

(14) Shoaee, S.; Subramaniyan, S.; Xin, H.; Keiderling, C.; Tuladhar, P. S.; Jamieson, F.; Jenekhe, S. A.; Durrant, J. R. Charge Photogeneration for a Series of Thiazolo-Thiazole Donor Polymers Blended with the Fullerene Electron Acceptors PCBM and ICBA. *Adv. Funct. Mater.* **2013**, *23*, 3286−3298.

(15) Li, G.; Shrotriya, V.; Huang, J.; Yao, Y.; Moriarty, T.; Emery, K.; Yang, Y. High-Efficiency Solution Processable Polymer Photovoltaic Cells by Self-Organization of Polymer Blends. *Nat. Mater.* **2005**, *4*, 864−868.

(16) Verploegen, E.; Mondal, R.; Bettinger, C. J.; Sok, S.; Toney, M. F.; Bao, Z. Effects of Thermal Annealing Upon the Morphology of Polymer-Fullerene Blends. *Adv. Funct. Mater.* **2010**, *20*, 3519−3529.

(17) Westacott, P.; Tumbleston, J. R.; Shoaee, S.; Fearn, S.; Bannock, J. H.; Gilchrist, J. B.; Heutz, S.; DeMello, J.; Heeney, M.; Ade, H.; et al.

On the Role of Intermixed Phases in Organic Photovoltaic Blends. *Energy Environ. Sci.* **2013**, *6*, 2756−2764.
(18) Gomez, E. D.; Barteau, K. P.; Wang, H.; Toney, M. F.; Loo, Y.-L. Correlating the Scattered Intensities of P3HT and PCBM to the Current Densities of Polymer Solar Cells. *Chem. Commun. (Camb.)* **2011**, *47*, 436−438.
(19) Guo, J.; Ohkita, H.; Benten, H.; Ito, S. Charge Generation and Recombination Dynamics in Poly (3-Hexylthiophene)/fullerene Blend Films with Different Regioregularities and Morphologies. *J. Am. Chem. Soc.* **2010**, *132*, 6154−6164.
(20) Cates, N. C.; Gysel, R.; Beiley, Z.; Miller, C. E.; Toney, M. F.; Heeney, M.; McCulloch, I.; McGehee, M. D. Tuning the Properties of Polymer Bulk Heterojunction Solar Cells by Adjusting Fullerene Size to Control Intercalation. *Nano Lett.* **2009**, *9*, 4153−4157.
(21) Watts, B.; Belcher, W. J.; Thomsen, L.; Ade, H.; Dastoor, P. C. A Quantitative Study of PCBM Diffusion during Annealing of P3HT:PCBM Blend Films. *Macromolecules* **2009**, *42*, 8392−8397.
(22) Peet, J.; Soci, C.; Coffin, R. C.; Nguyen, T. Q.; Mikhailovsky, A.; Moses, D.; Bazan, G. C. Method for Increasing the Photoconductive Response in Conjugated Polymer/fullerene Composites. *Appl. Phys. Lett.* **2006**, *89*, 252103−252105.
(23) Peet, J.; Kim, J.; Coates, N.; Ma, W. L.; Moses, D.; Heeger, A. J.; Bazan, G. C. Efficiency Enhancement in Low-Bandgap Polymer Solar Cells by Processing with Alkane Dithiols. *Nat. Mater.* **2007**, *6*, 497−500.
(24) Lee, J. K.; Ma, W. L.; Brabec, C. J.; Yuen, J.; Moon, J. S.; Kim, J. Y.; Lee, K.; Bazan, G. C.; Heeger, A. J. Processing Additives for Improved Efficiency from Bulk Heterojunction Solar Cells. *J. Am. Chem. Soc.* **2008**, *130*, 3619−3623.
(25) Chang, L.; Jacobs, I. E.; Augustine, M. P.; Moulé, A. J. Correlating Dilute Solvent Interactions to Morphology and OPV Device Performance. *Org. Electron.* **2013**, *14*, 2431−2443.
(26) Chen, W.; Xu, T.; He, F.; Wang, W.; Wang, C.; Strzalka, J.; Liu, Y.; Wen, J.; Miller, D. J.; Chen, J.; et al. Hierarchical Nanomorphologies Promote Exciton Dissociation in Polymer/fullerene Bulk Heterojunction Solar Cells. *Nano Lett.* **2011**, *11*, 3707−3713.
(27) Ayzner, A. L.; Tassone, C. J.; Tolbert, S. H.; Schwartz, B. J. Reappraising the Need for Bulk Heterojunctions in Polymer−Fullerene Photovoltaics: The Role of Carrier Transport in All-Solution-Processed P3HT/PCBM Bilayer Solar. *J. Phys. Chem. C* **2009**, *113*, 20050−20060.
(28) Chen, D.; Liu, F.; Wang, C.; Nakahara, A.; Russell, T. P. Bulk Heterojunction Photovoltaic Active Layers via Bilayer. *Nano Lett.* **2011**, *11*, 2071−2078.
(29) Gevaerts, V. S.; Koster, L. J. A.; Wienk, M. M.; Janssen, R. A. J. Discriminating between Bilayer and Bulk Heterojunction Polymer:-Fullerene Solar Cells Using the External Quantum Efficiency. *ACS Appl. Mater. Interfaces* **2011**, *3*, 3252−3255.
(30) Moon, J. S.; Takacs, C. J.; Sun, Y.; Heeger, A. J. Spontaneous Formation of Bulk Heterojunction Nanostructures: Multiple Routes to Equivalent Morphologies. *Nano Lett.* **2011**, *11*, 1036−1039.
(31) Cho, S.-M.; Bae, J.-H.; Jang, E.; Kim, M.-H.; Lee, C.; Lee, S.-D. Solvent Effect of the Fibrillar Morphology on the Power Conversion Efficiency of a Polymer Photovoltaic Cell in a Diffusive Heterojunction. *Semicond. Sci. Technol.* **2012**, *27*, 125018.
(32) Gadisa, A.; Tumbleston, J. R.; Ko, D.-H.; Aryal, M.; Lopez, R.; Samulski, E. T. The Role of Solvent and Morphology on Miscibility of Methanofullerene and poly(3-Hexylthiophene). *Thin Solid Films* **2012**, *520*, 5466−5471.
(33) Thummalakunta, L. N. S. A.; Yong, C. H.; Ananthanarayanan, K.; Luther, J. P3HT Based Solution-Processed Pseudo Bi-Layer Organic Solar Cell with Enhanced Performance. *Org. Electron.* **2012**, *13*, 2008−2016.
(34) Wong, M. K.; Wong, K. Y. Investigation of the Factors Affecting the Power Conversion Efficiency of All-Solution-Processed "bilayer" P3HT:PCBM Solar Cells. *Synth. Met.* **2013**, *170*, 1−6.
(35) Li, H.; Qi, Z.; Wang, J. Layer-by-Layer Processed Polymer Solar Cells with Self-Assembled Electron Buffer Layer. *Appl. Phys. Lett.* **2013**, *102*, 213901.
(36) Yang, B.; Yuan, Y.; Huang, J. Reduced Bimolecular Charge Recombination Loss in Thermally-Annealed Bilayer Heterojunction Photovoltaic Devices with Large External Quantum Efficiency and Fill Factor. *J. Phys. Chem. C* **2014**, *118*, 5196−5202.
(37) Lin, Y.; Ma, L.; Li, Y.; Liu, Y.; Zhu, D.; Zhan, X. Small-Molecule Solar Cells with Fill Factors up to 0.75 via a Layer-by-Layer Solution Process. *Adv. Energy Mater.* **2014**, *4*, 1300626.
(38) Nardes, A. M.; Ayzner, A. L.; Hammond, S. R.; Ferguson, A. J.; Schwartz, B. J.; Kopidakis, N. Photoinduced Charge Carrier Generation and Decay in Sequentially Deposited Polymer/Fullerene Layers: Bulk Heterojunction vs Planar Interface. *J. Phys. Chem. C* **2012**, *116*, 7293−7305.
(39) Lee, K. H.; Schwenn, P. E.; Smith, A. R. G.; Cavaye, H.; Shaw, P. E.; James, M.; Krueger, K. B.; Gentle, I. R.; Meredith, P.; Burn, P. L. Morphology of All-Solution-Processed "Bilayer" Organic Solar Cells. *Adv. Mater.* **2011**, *23*, 766−770.
(40) Treat, N. D.; Brady, M. A.; Smith, G.; Toney, M. F.; Kramer, E. J.; Hawker, C. J.; Chabinyc, M. L. Interdiffusion of PCBM and P3HT Reveals Miscibility in a Photovoltaically Active Blend. *Adv. Energy Mater.* **2011**, *1*, 82−89.
(41) Lee, K. H.; Zhang, Y.; Burn, P. L.; Gentle, I. R.; James, M.; Nelson, A.; Meredith, P. Correlation of Diffusion and Performance in Sequentially Processed P3HT/PCBM Heterojunction Films by Time-Resolved Neutron Reflectometry. *J. Mater. Chem. C* **2013**, *1*, 2593−2598.
(42) Hawks, S. A.; Aguirre, J. C.; Schelhas, L. T.; Thompson, R. J.; Huber, R. C.; Ferreira, A. S.; Zhang, G.; Herzing, A. A.; Tolbert, S. H.; Schwartz, B. J. Comparing Matched Polymer:Fullerene Solar Cells Made by Solution-Sequential Processing and Traditional Blend Casting: Nanoscale Structure and Device Performance. *J. Phys. Chem. C* **2014**, DOI: 10.1021/jp504560r.
(43) Dang, M.; Hirsch, L.; Wantz, G. P3HT: PCBM, Best Seller in Polymer Photovoltaic Research. *Adv. Mater.* **2011**, *23*, 3597−3602.
(44) Yang, C.; Heeger, A. Morphology of Composites of Semiconducting Polymers Mixed with C 60. *Synth. Met.* **1996**, *83*, 85−88.
(45) Wang, D. H.; Moon, J. S.; Seifter, J.; Jo, J.; Park, J. H.; Park, O. O.; Heeger, A. J. Sequential Processing: Control of Nanomorphology in Bulk Heterojunction Solar Cells. *Nano Lett.* **2011**, *11*, 3163−3168.
(46) Li, H.; Li, Y.; Wang, J. Optimizing Performance of Layer-by-Layer Processed Polymer Solar Cells. *Appl. Phys. Lett.* **2012**, *101*, 033907.
(47) Li, H.; Wang, J. Layer-by-Layer Processed High-Performance Polymer Solar Cells. *Appl. Phys. Lett.* **2012**, *101*, 263901−263905.
(48) Cheng, P.; Hou, J.; Li, Y.; Zhan, X. Layer-by-Layer Solution-Processed Low-Bandgap Polymer-PC 61 BM Solar Cells with High Efficiency. *Adv. Energy Mater.* **2014**, DOI: 10.1002/aenm.201301349.
(49) Loiudice, A.; Rizzo, A.; Latini, G.; Nobile, C.; de Giorgi, M.; Gigli, G. Graded Vertical Phase Separation of Donor/acceptor Species for Polymer Solar Cells. *Sol. Energy Mater. Sol. Cells* **2012**, *100*, 147−152.
(50) Loiudice, A.; Rizzo, A.; Biasiucci, M.; Gigli, G. Bulk Heterojunction versus Diffused Bilayer: The Role of Device Geometry in Solution P-Doped Polymer-Based Solar Cells. *J. Phys. Chem. Lett.* **2012**, *3*, 1908−1915.
(51) Tao, C.; Aljada, M.; Shaw, P. E.; Lee, K. H.; Cavaye, H.; Balfour, M. N.; Borthwick, R. J.; James, M.; Burn, P. L.; Gentle, I. R.; et al. Controlling Hierarchy in Solution-Processed Polymer Solar Cells Based on Crosslinked P3HT. *Adv. Energy Mater.* **2013**, *3*, 105−112.
(52) Yang, H. Y.; Kang, N. S.; Hong, J.-M.; Song, Y.-W.; Kim, T. W.; Lim, J. A. Efficient Bilayer Heterojunction Polymer Solar Cells with Bumpy Donor−acceptor Interface Formed by Facile Polymer Blend. *Org. Electron.* **2012**, *13*, 2688−2695.
(53) Chen, H.; Hu, S.; Zang, H.; Hu, B.; Dadmun, M. Precise Structural Development and Its Correlation to Function in Conjugated Polymer: Fullerene Thin Films by Controlled Solvent Annealing. *Adv. Funct. Mater.* **2013**, *23*, 1701−1710.
(54) Kim, D. H.; Mei, J.; Ayzner, A. L.; Schmidt, K.; Giri, G.; Appleton, A. L.; Toney, M. F.; Bao, Z. Sequentially Solution-

Processed, Nanostructured Polymer Photovoltaics Using Selective Solvents. *Energy Environ. Sci.* **2014**, *7*, 1103−1109.
(55) Ayzner, A. L.; Doan, S. C.; Tremolet de Villers, B.; Schwartz, B. J. Ultrafast Studies of Exciton Migration and Polaron Formation in Sequentially Solution-Processed Conjugated Polymer/Fullerene Quasi-Bilayer Photovoltaics. *J. Phys. Chem. Lett.* **2012**, *3*, 2281−2287.
(56) Rochester, C. W.; Mauger, S. A.; Moule, A. J. Investigating the Morphology of Polymer/Fullerene Layers Coated Using Orthogonal Solvents. *J. Phys. Chem. C* **2012**, *116*, 7287−7292.
(57) Jiang, X.; Osterbacka, R.; Korovyanko, O.; An, C. P.; Horovitz, B.; Janssen, R. A. J.; Vardeny, Z. V. Spectroscopic Studies of Photoexcitations in Regioregular and Regiorandom Polythiophene Films. *Adv. Funct. Mater.* **2002**, *12*, 587−597.
(58) Kim, Y.; Cook, S.; Tuladhar, S. M.; Choulis, S. A.; Nelson, J.; Durrant, J. R.; Bradley, D. D. C.; Giles, M.; McCulloch, I.; Ha, C.-S.; et al. A Strong Regioregularity Effect in Self-Organizing Conjugated Polymer Films and High-Efficiency Polythiophene:fullerene Solar Cells. *Nat. Mater.* **2006**, *5*, 197−203.
(59) Mauer, R.; Kastler, M.; Laquai, F. The Impact of Polymer Regioregularity on Charge Transport and Efficiency of P3HT:PCBM Photovoltaic Devices. *Adv. Funct. Mater.* **2010**, *20*, 2085−2092.
(60) Adachi, T.; Brazard, J.; Ono, R. J.; Hanson, B.; Traub, M. C.; Wu, Z.; Li, Z.; Bolinger, J. C.; Ganesan, V.; Bielawski, C. W.; et al. Regioregularity and Single Polythiophene Chain Conformation. *J. Phys. Chem. Lett.* **2011**, *2*, 1400−1404.
(61) Collins, B. A.; Tumbleston, J. R.; Ade, H. Miscibility, Crystallinity, and Phase Development in P3HT/PCBM Solar Cells: Toward an Enlightened Understanding of Device Morphology and Stability. *J. Phys. Chem. Lett.* **2011**, *2*, 3135−3145.
(62) Brown, P. J.; Thomas, D. S.; Köhler, A.; Wilson, J. S.; Kim, J.-S.; Ramsdale, C. M.; Sirringhaus, H.; Friend, R. H. Effect of Interchain Interactions on the Absorption and Emission of poly(3-Hexylthiophene). *Phys. Rev. B* **2003**, *67*, 064203−064218.
(63) Kohn, P.; Rong, Z.; Scherer, K. H.; Sepe, A.; Sommer, M.; Müller-Buschbaum, P.; Friend, R. H.; Steiner, U.; Hüttner, S. Crystallization-Induced 10-Nm Structure Formation in P3HT/PCBM Blends. *Macromolecules* **2013**, *46*, 4002−4013.
(64) Bronstein, H. A.; Luscombe, C. K. Externally Initiated Regioregular P3HT with Controlled Molecular Weight and Narrow Polydispersity. *J. Am. Chem. Soc.* **2009**, *131*, 12894−12895.
(65) Brabec, C. J.; Heeney, M.; McCulloch, I.; Nelson, J. Influence of Blend Microstructure on Bulk Heterojunction Organic Photovoltaic Performance. *Chem. Soc. Rev.* **2011**, *40*, 1185−1199.
(66) Kline, R. J.; McGehee, M. D.; Kadnikova, E. N.; Liu, J.; Fréchet, J. M. J.; Toney, M. F. Dependence of Regioregular Poly (3-Hexylthiophene) Film Morphology and Field-Effect Mobility on Molecular Weight. *Macromolecules* **2005**, *38*, 3312−3319.
(67) Zhang, R.; Li, B.; Iovu, M. C.; Jeffries-el, M.; Cooper, J.; Jia, S.; Tristram-nagle, S.; Smilgies, D. M.; Lambeth, D. N.; Mccullough, R. D.; et al. Nanostructure Dependence of Field-Effect Mobility in Regioregular poly(3-Hexylthiophene) Thin Film Field Effect Transistors. *J. Am. Chem. Soc.* **2006**, *128*, 3480−3481.
(68) Noriega, R.; Rivnay, J.; Vandewal, K.; Koch, F. P. V; Stingelin, N.; Smith, P.; Toney, M. F.; Salleo, A. A General Relationship between Disorder, Aggregation and Charge Transport in Conjugated Polymers. *Nat. Mater.* **2013**, *12*, 1038−1044.
(69) Pingel, P.; Zen, A.; Abellón, R. D.; Grozema, F. C.; Siebbeles, L. D. A.; Neher, D. Temperature-Resolved Local and Macroscopic Charge Carrier Transport in Thin P3HT Layers. *Adv. Funct. Mater.* **2010**, *20*, 2286−2295.
(70) Brinkmann, M.; Rannou, P. Molecular Weight Dependence of Chain Packing and Semicrystalline Structure in Oriented Films of Regioregular Poly(3-Hexylthiophene) Revealed by High-Resolution Transmission Electron Microscopy. *Macromolecules* **2009**, *42*, 1125−1130.
(71) Kline, R. J.; McGehee, M. D.; Kadnikova, E. N.; Liu, J.; Fréchet, J. M. J. Controlling the Field-Effect Mobility of Regioregular Polythiophene by Changing the Molecular Weight. *Adv. Mater.* **2003**, *15*, 1519−1522.
(72) Müller, C.; Ferenczi, T. a. M.; Campoy-Quiles, M.; Frost, J. M.; Bradley, D. D. C.; Smith, P.; Stingelin-Stutzmann, N.; Nelson, J. Binary Organic Photovoltaic Blends: A Simple Rationale for Optimum Compositions. *Adv. Mater.* **2008**, *20*, 3510−3515.
(73) Baek, W.-H.; Yoon, T.-S.; Lee, H. H.; Kim, Y.-S. Composition-Dependent Phase Separation of P3HT:PCBM Composites for High Performance Organic Solar Cells. *Org. Electron.* **2010**, *11*, 933−937.
(74) Van Bavel, S. S.; Bärenklau, M.; de With, G.; Hoppe, H.; Loos, J. P3HT/PCBM Bulk Heterojunction Solar Cells: Impact of Blend Composition and 3D Morphology on Device Performance. *Adv. Funct. Mater.* **2010**, *20*, 1458−1463.
(75) Kirchartz, T.; Deledalle, F.; Tuladhar, P. S.; Durrant, J. R.; Nelson, J. On the Differences between Dark and Light Ideality Factor in Polymer: Fullerene Solar Cells. *J. Phys. Chem. Lett.* **2013**, *4*, 2371−2376.
(76) Street, R. A.; Krakaris, A.; Cowan, S. R. Recombination Through Different Types of Localized States in Organic Solar Cells. *Adv. Funct. Mater.* **2012**, *22*, 4608−4619.
(77) Street, R. A.; Schoendorf, M.; Roy, A.; Lee, J. H. Interface State Recombination in Organic Solar Cells. *Phys. Rev. B* **2010**, *81*, 205307.
(78) Kirchartz, T.; Pieters, B. E.; Kirkpatrick, J.; Rau, U.; Nelson, J. Recombination via Tail States in Polythiophene:fullerene Solar Cells. *Phys. Rev. B* **2011**, *83*, 115209.
(79) Foertig, A.; Rauh, J.; Dyakonov, V.; Deibel, C. Shockley Equation Parameters of P3HT:PCBM Solar Cells Determined by Transient Techniques. *Phys. Rev. B* **2012**, *86*, 115302.
(80) Woo, C. H.; Thompson, B. C.; Kim, B. J.; Toney, M. F.; Fréchet, J. M. J. The Influence of poly(3-Hexylthiophene) Regioregularity on Fullerene-Composite Solar Cell Performance. *J. Am. Chem. Soc.* **2008**, *130*, 16324−16329.
(81) Veldman, D.; Meskers, S. C. J.; Janssen, R. A. J. The Energy of Charge-Transfer States in Electron Donor-Acceptor Blends: Insight into the Energy Losses in Organic Solar Cells. *Adv. Funct. Mater.* **2009**, *19*, 1939−1948.
(82) Tress, W.; Leo, K.; Riede, M. Optimum Mobility, Contact Properties, and Open-Circuit Voltage of Organic Solar Cells: A Drift-Diffusion Simulation Study. *Phys. Rev. B* **2012**, *85*, 155201.
(83) Clark, J.; Silva, C.; Friend, R. H.; Spano, F. C. Role of Intermolecular Coupling in the Photophysics of Disordered Organic Semiconductors: Aggregate Emission in Regioregular Polythiophene. *Phys. Rev. Lett.* **2007**, *98*, 206406.
(84) Spano, F. C. Modeling Disorder in Polymer Aggregates: The Optical Spectroscopy of Regioregular poly(3-Hexylthiophene) Thin Films. *J. Chem. Phys.* **2005**, *122*, 234701.
(85) Gierschner, J.; Mack, H.-G.; Lüer, L.; Oelkrug, D. Fluorescence and Absorption Spectra of Oligophenylenevinylenes: Vibronic Coupling, Band Shapes, and Solvatochromism. *J. Chem. Phys.* **2002**, *116*, 8596.
(86) Niles, E. T.; Roehling, J. D.; Yamagata, H.; Wise, A. J.; Spano, F. C.; Moule, A. J.; Grey, J. K. J-Aggregate Behavior in Poly-3-Hexylthiophene Nanofibers. *J. Phys. Chem. Lett.* **2012**, *3*, 259−263.
(87) Gao, Y.; Grey, J. K. Resonance Chemical Imaging of Polythiophene/fullerene Photovoltaic Thin Films: Mapping Morphology-Dependent Aggregated and Unaggregated C═C Species. *J. Am. Chem. Soc.* **2009**, *131*, 9654−9662.
(88) O'Connor, B. T.; Reid, O. G.; Zhang, X.; Kline, R. J.; Richter, L. J.; Gundlach, D. J.; DeLongchamp, D. M.; Toney, M. F.; Kopidakis, N. Rumbles, G. Morphological Origin of Charge Transport Anisotropy in Aligned Polythiophene Thin Films. *Adv. Funct. Mater.* **2014**, DOI: 10.1002/adfm.201303351.
(89) Reid, O.; Pensack, R.; Song, Y. Charge Photogeneration in Neat Conjugated Polymers. *Chem. Mater.* **2013**, DOI: 10.1021/cm4027144.
(90) Lee, K. H.; Schwenn, P. E.; Smith, A. R. G.; Cavaye, H.; Shaw, P. E.; James, M.; Krueger, K. B.; Gentle, I. R.; Meredith, P.; Burn, P. L. Morphology of All-Solution-Processed "Bilayer" Organic Solar Cells. *Adv. Mater.* **2011**, *23*, 766−770.
(91) Abbas, M.; Tekin, N. Balanced Charge Carrier Mobilities in Bulk Heterojunction Organic Solar Cells. *Appl. Phys. Lett.* **2012**, *101*, 073302.

(92) Kumar, A.; Liao, H.-H.; Yang, Y. Hole Mobility in Optimized Organic Photovoltaic Blend Films Obtained Using Extraction Current Transients. *Org. Electron.* **2009**, *10*, 1615−1620.
(93) Yin, W.; Dadmun, M. A New Model for the Morphology of P3HT/PCBM Organic Photovoltaics from Small-Angle Neutron Scattering: Rivers and Streams. *ACS Nano* **2011**, 4756−4768.
(94) Chen, H.; Hegde, R.; Browning, J.; Dadmun, M. D. The Miscibility and Depth Profile of PCBM in P3HT: Thermodynamic Information to Improve Organic Photovoltaics. *Phys. Chem. Chem. Phys.* **2012**, *14*, 5635−5641.
(95) Kozub, D. R.; Vakhshouri, K.; Orme, L. M.; Wang, C.; Hexemer, A.; Gomez, E. D. Polymer Crystallization of Partially Miscible Polythiophene/Fullerene Mixtures Controls Morphology. *Macromolecules* **2011**, *44*, 5722−5726.
(96) Chen, W.; Nikiforov, M. P.; Darling, S. B. Morphology Characterization in Organic and Hybrid Solar Cells. *Energy Environ. Sci.* **2012**, *5*, 8045−8074.